Citation: Cell Death and Disease (2012) 3, e266; doi:10.1038/cddis.2012.6

www.nature.com/cddis

The *EIF4EBP3* translational repressor is a marker of *CDC73* tumor suppressor haploinsufficiency in a parathyroid cancer syndrome

J-H Zhang[1], EM Seigneur[1], M Pandey[1], A Loshakov[1], PK Dagur[2], PS Connelly[3], L Koo[4], LM Panicker[1,5] and WF Simonds*[,1]

Germline mutation of the tumor suppressor gene *CDC73* confers susceptibility to the hyperparathyroidism-jaw tumor syndrome associated with a high risk of parathyroid malignancy. Inactivating *CDC73* mutations have also been implicated in sporadic parathyroid cancer, but are rare in sporadic benign parathyroid tumors. The molecular pathways that distinguish malignant from benign parathyroid transformation remain elusive. We previously showed that a hypomorphic allele of *hyrax (hyx)*, the *Drosophila* homolog of *CDC73*, rescues the loss-of-ventral-eye phenotype of *lobe*, encoding the fly homolog of Akt1s1/ PRAS40. We report now an interaction between *hyx* and *Tor*, a central regulator of cell growth and autophagy, and show that eukaryotic translation initiation factor 4E-binding protein (*EIF4EBP*), a translational repressor and effector of mammalian target of rapamycin (mTOR), is a conserved target of *hyx/CDC73*. Flies heterozygous for *Tor* and *hyx*, but not *Mnn1*, the homolog of the multiple endocrine neoplasia type 1 (*MEN1*) tumor suppressor associated with benign parathyroid tumors, are starvation resistant with reduced basal levels of *Thor/4E-BP*. Human peripheral blood cell levels of *EIF4EBP3* were reduced in patients with *CDC73*, but not *MEN1*, heterozygosity. Chromatin immunoprecipitation demonstrated occupancy of *EIF4EBP3* by endogenous parafibromin. These results show that *EIF4EBP3* is a peripheral marker of *CDC73* function distinct from *MEN1*-regulated pathways, and suggest a model whereby starvation resistance and/or translational de-repression contributes to parathyroid malignant transformation.

Cell Death and Disease (2012) **3,** 266; doi:10.1038/cddis.2012.6; published online 2 February 2012
Subject Category: Cancer

Germline loss-of-function mutation of the tumor suppressor gene *CDC73* (also known as *HRPT2*) confers susceptibility to the hyperparathyroidism-jaw tumor syndrome (HPT-JT), an autosomal dominant familial cancer syndrome associated with a high risk of parathyroid malignancy.[1–6] Analysis of multiple kindreds with HPT–JT by Carpten *et al*.[7] led to the identification of *CDC73/HRPT2* by positional candidate cloning. Inactivating somatic and/or germline *CDC73/HRPT2* mutations have also been implicated in sporadic parathyroid cancer.[8,9] *CDC73* encodes parafibromin,[7] a 531-amino acid putative tumor suppressor protein with sequence homology to yeast Cdc73p.[10] As was originally shown in yeast for Cdc73p,[11] evidence in humans suggests that parafibromin interacts with RNA polymerase II as a part of the PAF1 complex.[12–14] The components of the PAF1 complex are highly conserved in *Drosophila* as well, including *hyrax* (*hyx*) a homolog of *CDC73.*[15]

Despite its strong association with parathyroid cancer, inactivation of *CDC73* is quite rare in sporadic, benign parathyroid tumors.[16,17] In contrast, inactivation of the multiple endocrine neoplasia type 1 (*MEN1*) tumor suppressor gene is nearly always associated with benign parathyroid tumors in the context of familial or sporadic MEN1,[18] and somatic inactivation of *MEN1* in sporadic benign parathyroid tumors is common.[19,20] Despite the identification of these key parathyroid tumor suppressor genes, the mechanisms and pathways that distinguish benign from malignant transformation of the parathyroid remain elusive. Furthermore, the development of a *Cdc73/Hrpt2* knockout mouse model[21] and other experimental approaches[15,22,23] have so far yielded little insight into the pathway(s) whereby *CDC73* loss-of-function might promote tumorigenesis.

Using *Drosophila* as a model system, we recently showed that *hyx* mutant flies were resistant to starvation and that *hyx*

[1]Metabolic Diseases Branch, National Institute of Diabetes and Digestive and Kidney Diseases, National Institute of Allergy and Infectious Diseases, National Institutes of Health, Bethesda, MD, USA; [2]Flow Cytometry Core Facility, National Institute of Allergy and Infectious Diseases, National Institutes of Health, Bethesda, MD, USA; [3]Electron Microscopy Core Facility, National Heart, Lung and Blood Institute, National Institute of Allergy and Infectious Diseases, National Institutes of Health, Bethesda, MD, USA and [4]Research Technologies Branch, National Institute of Allergy and Infectious Diseases, National Institutes of Health, Bethesda, MD, USA
*Corresponding author: WF Simonds, Metabolic Diseases Branch, National Institutes of Health, Building 10, Room 8C-101, 10 Center Dr. MSC 1752, Bethesda, MD 20892-1752, USA. Tel: +1 301 496 9299; Fax: +1 301 402 0374; E-mail: wfs@helix.nih.gov
[5]Present address: Department of Microbiology and Immunology, University of Maryland School of Medicine, 660 West Redwood Street, Howard Hall, Room 319C, Baltimore, MD 21201, USA.
Keywords: PAF1 complex; *HRPT2*; apoptosis; eIF4E; 4E-BP; s6k
Abbreviations: HPT-JT, hyperparathyroidism-jaw tumor syndrome; Hyx, hyrax; EIF4EBP, eukaryotic translation initiation factor 4E-binding protein; MEN1, multiple endocrine neoplasia type 1; PRAS40, proline-rich AKT substrate of 40 kDa; AKT1S1, Akt1 substrate 1; mTOR, mammalian target of rapamycin; FBS, fetal bovine serum; APF, after pupal formation; TUNEL, terminal deoxynucleotidyl transferase mediated dUTP nick end labeling; ChIP, chromatin immunoprecipitation; WBC, cultured human peripheral blood mononuclear cells
Received 18.7.11; revised 19.12.11; accepted 09.1.12; Edited by A Stephanou

rescued the loss-of-ventral-eye phenotype of *lobe*, the fly homolog of Akt1 substrate 1 (*AKT1S1*).[24] Akts1, also called 40 kDa proline-rich AKT substrate (PRAS40), is a negative regulator of mammalian target of rapamycin (mTOR) complex 1.[25] The protein kinase mTOR functions as a cellular sensor of nutrient and energy availability, and regulates cell growth and autophagy.[26]

One well-characterized effector of mTOR is the eukaryotic translation initiation factor 4E-binding protein (eIF4EBP or 4E-BP) that competes with eIF-4G for binding to eIF-4E to inhibit mRNA cap-dependent translational initiation.[27,28] Phosphorylation of eIF4EBP by mTOR reduces its affinity for eIF-4E and promotes the initiation of protein synthesis from a pool of transcripts enriched in mRNAs encoding proteins involved in angiogenesis, growth, and survival.[29] Enhanced function of eIF-4E, often a result of inactivation of eIF4EBP by phosphorylation, is linked to poor prognosis, tumor progression, and metastasis in squamous cell,[30] breast,[31,32] ovarian, [33] and other cancers.

We demonstrate now that *EIF4EBP* is an evolutionarily conserved target of *hyx/CDC73,* and show that basal and serum starvation-stimulated levels of *EIF4EBP3* transcript are reduced in peripheral mononuclear cells from patients heterozygous for *CDC73*, but not *MEN1*. We show that the expression of the *EIF4EBP3* translational repressor represents a peripheral marker of *CDC73* function and propose a model whereby starvation resistance, mediated at least in part by de-repression of protein translation, may contribute to parathyroid malignant transformation.

Results

We previously showed that in *Drosophila* a hypomorphic allele of *hyx* rescues the eye phenotype of *lobe* and that *hyx* heterozygous flies were resistant to starvation.[24] Thus, $L^{si}/+$; $hyx^{EY6898}/+$ double heterozygotes have normal eyes, even though heterozygous $L^{si/+}$ flies show a loss-of-ventral-eye phenotype (Figure 1e, cf. 1a–c), and provide a sensitive genetic background to identify additional genes that interact with *L*, *hyx*, or both by eye phenotype screening.[24]

On the basis of the rescue of *lobe* by *hyx* and the enhanced resistance to starvation seen in *hyx* heterozygous flies,[24] we used the eye phenotype screening assay to look for an interaction of *hyx* with *Tor*, a key regulator of cellular nutritional homeostasis[26] and target of *lobe/ Akt1S1/ PRAS40* inhibition.[25] To this end we crossed doubly heterozygous ($L^{si}/+$; $hyx^{EY6898}/+$) flies with a $Tor^{MB07988}$ mutant strain (Figures 1h–q, s, and t; Table 1). Approximately, 40% of the triple heterozygote ($L^{si}/Tor^{MB07988}$ $hyx^{EY6898}/+$) flies had NOG eye phenotypes (notch and dysplastic overgrowth), including half eyes with dysplastic overgrowths[24] (Figures 1h–k; Table 1, cross 8). The overgrowths typically appeared in or near the missing ventral eye region (Figures 1i–q). The ommatidia and the sensory bristles were deformed and in disarray (Figures 1s and t, cf. 1r). Testing of another *Tor* mutant allele, Tor^{K17004}, gave similar results (Table 1, cross 10). In contrast, 90% or more of the doubly heterozygous mutant flies carrying the L^{si} allele ($L^{si}/Tor^{MB07988}$ L^{si}/Tor^{K17004} $L^{si}/+$;$hyx^{EY6898}/+$) had normal eyes (Figures 1e and f; Table 1, crosses 3, 7, and 11). As the other possible doubly heterozygous mutant combinations from the same matings produced flies with normal eyes (Figure 1g; Table 1, crosses 9 and 12), the observed strong eye phenotype must result from the specific combination of *hyx* and *Tor* loss-of-function.

We previously showed that the eye discs of $L^{si}/+$; $hyx^{EY6898}/orb2^{BG02373}$ triple heterozygotes with a propensity to later develop the NOG phenotype were characterized by an abnormal pattern of apoptosis at the larval stage.[24] In contrast, the larval eye discs of $L^{si}/Tor^{MB07988}$ $hyx^{EY6898}/+$ triple heterozygotes showed no gross abnormalities in the pattern or extent of apoptosis compared with w^{1118} controls (data not shown).

We, therefore, compared the pupal eye discs of wild-type and $L^{si}/Tor^{MB07988}$ $hyx^{EY6898}/+$ triple heterozygotes to look for developmental abnormalities that might account for the subsequent development of the NOG phenotype in the triple mutants. Normal eye development in *Drosophila* involves a wave of cell apoptosis between 35 and 50 h after pupation that eliminates a large fraction of undifferentiated interommatidial cells.[34] The pupal eye discs of wild-type and $L^{si}/Tor^{MB07988}$ $hyx^{EY6898}/+$ triple heterozygote flies were, therefore, examined at 45 h after pupation using the terminal deoxynucleotidyl transferase mediated dUTP nick end labeling (TUNEL) assay to identify the nuclei of cells undergoing apoptosis (Figure 2). Eye discs from $L^{si}/Tor^{MB07988}$ $hyx^{EY6898}/+$ triple heterozygote pupae showed a disordered pattern of apoptosis as well as a significant decrease in TUNEL-positive apoptotic nuclei compared with eyes from w^{1118} controls (Figures 2a and b). Thus, the eye discs of $L^{si}/Tor^{MB07988}$ $hyx^{EY6898}/+$ triple heterozygotes with a propensity to later develop the NOG phenotype were characterized by a substantial reduction in the usual burst of apoptosis between 35 and 50 h after pupation.

As current models suggest that Tor acts as a nutrient sensor, and regulator of cell growth and autophagy,[26] we studied starvation resistance in *Tor* and *hyx* mutant flies. Consistent with our previous results,[24] *hyx* heterozygous flies were resistant to starvation compared with w^{1118} controls (Figure 3a). Resistance to starvation was also found to be higher in *Tor* ($Tor^{MB07988}/+$) heterozygous flies (Figure 3b). Double *hyx/ Tor* heterozygotes ($Tor^{MB07988}/+$; $hyx^{EY6898}/+$) were also resistant to starvation without any obvious additivity of the effect (Figure 3c).

A separate set of experiments used a different mutant allele of *Tor* (Tor^{K17004}) and showed that $Tor^{K17004}/+$ heterozygotes, like $Tor^{MB07988}/+$ heterozygous flies, exhibited resistance to starvation (Figure 3d). A double *hyx/ Tor* heterozygote strain demonstrated comparable resistance to starvation as seen with the single heterozygotes (Figure 3e, cf. 3a and d). We tested for rescue of the phenotype exploiting the fact that *hyx* can be overexpressed in strains carrying the GAL4-sensitive hyx^{EY6898} allele by mating to *GAL4*-overexpressing strains.[15,24] As shown in Figure 3f, overexpression of *hyx* in flies carrying the ubiquitously expressed *act5C-Gal4* driver and doubly heterozygous for *hyx/ Tor* mutation restored starvation sensitivity to near control levels, whereas control flies with 5C-actin promoter-driven GAL4 expression only had slightly enhanced starvation resistance (Figure 3f). In contrast to the *hyx* mutants, flies heterozygous for *Mnn1* ($Mnn1^{DG30701}/+$) were sensitive to starvation like the w^{1118}

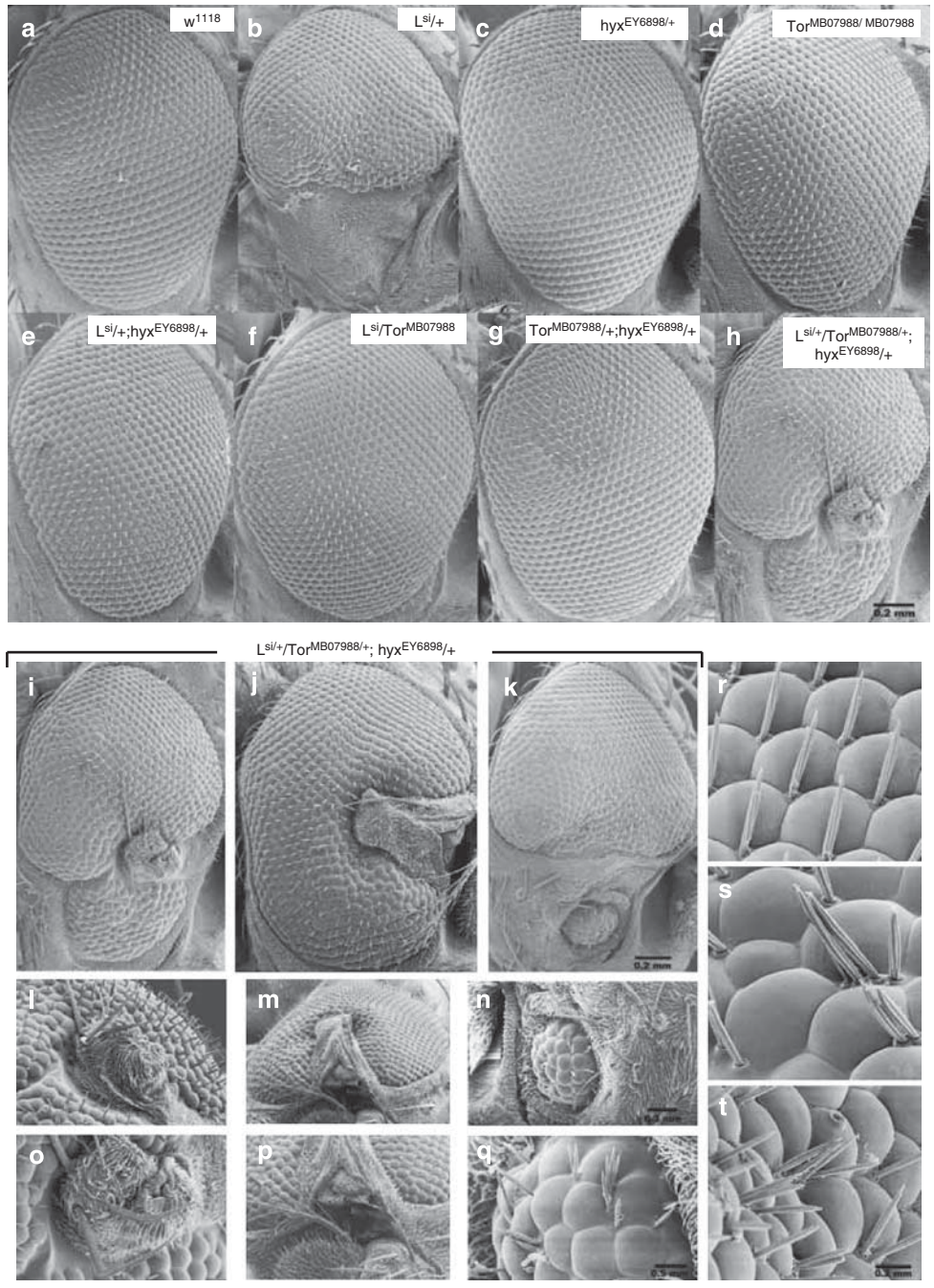

Figure 1 Genetic interaction among *lobe/Akt1s1*, *hyx/CDC73*, and *Tor* evident from *Drosophila* eye phenotypes. Genetic interactions were recognized by the formation of novel NOG structures at the ventral part of the adult eye after crosses between flies with different genotypes. Shown are representative eye phenotypes captured by scanning electron microscopy for w^{1118} control (**a**), heterozygous L^{si} mutant of *lobe*/*AKT1S1* (**b**), heterozygous hyx^{EY6898} mutant of *hyx/CDC73* (**c**), homozygous $Tor^{MB07988}$ mutant of *Tor* (**d**); double heterozygous mutants of *lobe* and *hyx/CDC73* (**e**), *lobe* and *Tor* (**f**), and *hyx/CDC73* and *Tor* (**g**); and triple heterozygous hybrid mutants of *lobe*, *hyx/CDC73* and *Tor* strains (**h**). Images of additional eyes from triple heterozygous hybrid mutants of *lobe*, *hyx/CDC73* and *Tor* strains are shown in (**j**) and (**k**) (image (**i**) is a duplicate of (**h**)). Higher magnification images of dysplastic overgrowth regions of (**i**–**k**) are shown in (**l**–**n**) and (**o**–**q**). Higher magnification images of the ommatidial and sensory bristle phenotype of the triple heterozygous *lobe*, *hyx/CDC73* and *Tor* mutant are shown (**s** and **t**), with corresponding image of wild-type (**r**)

controls (Figure 3g). Thus, heterozygosity of *hyx* and *Tor*, but not *Mnn1*, confers starvation resistance. Furthermore, *hyx* gene overexpression, at least at time points <100 h in a model system using the GAL4-sensitive hyx^{EY6898} allele and the *act5C-Gal4* driver, can rescue the starvation-resistant phenotype of *Tor*.

To better understand the interaction between *hyx* and *Tor*, quantitative RT-PCR was used to measure transcript levels in *hyx* or *Tor* mutant fly strains. Levels of *hyx* transcript were partially reduced in $Tor^{MB07988}$ heterozygotes and by some 30% in $Tor^{MB07988}$ homozygotes compared to with control (Figure 4a). In contrast, adult flies heterozygous for hyx^{EY6898}

Table 1 Genetic interactions of *L*, *hyrax*, and *Tor*

Cross No.	Parent 1	Parent 2	F1 genotype	% flies with NOG[a] eye phenotype	% NOG in both eyes	% notch w/o OG	Molecular function
1	w^{1118}	w^{1118}	w^{1118}	0	0	0	
2	$L^{si/si}$	w^{1118}	$L^{si}/+$	0	0	100	*L* (*lobe*) is the fly homolog of mammalian *AKT1S1* (also called *PRAS40*)
3		$hyx^{EY6898}/+$	$L^{si}/+;hyx^{EY6898}/+$	6	0	11	*Hyx (hyrax)* is the fly homolog of *CDC73/ HRPT2*
4	$hyx^{EY6898}/+$	w^{1118}	$hyx^{EY6898}/+$	0	0	0	
5	$Tor^{MB07988/MB07988}$	$Tor^{MB07988/MB07988}$	$Tor^{MB07988/MB07988}$	0	0	0	*Tor* is a key cellular kinase involved in the regulation of cell growth and nutritional homeostasis
6		w^{1118}	$Tor^{MB07988}/+$	0	0	0	
7		$L^{si}/+$	$L^{si}/Tor^{MB07988}$	6	0	2	
8		$L^{si}/+;hyx^{EY6898}/+$	$L^{si}/Tor^{MB07988}; hyx^{EY6898}/+$	40***	7	3	
9		$hyx^{EY6898}/+$	$Tor^{MB07988}/+; hyx^{EY6898}/+$	0	0	0	
10	$Tor^{K17004}/+$	$L^{si}/+; hyx^{EY6898}/+$	$L^{si}/Tor^{K17004}; hyx^{EY6898}/+$	45***	8	7	
11			L^{si}/Tor^{K17004}	10	<1	9	
12		$hyx^{EY6898}/+$	$Tor^{K17004}/+; hyx^{EY6898}/+$	0	0	0	

[a]NOG: notch and overgrowth (OG), with notches and variably sized dysplastic overgrowths in the ventral eye fields. ***$P<0.0001$ compared with w1118n, and all double and single heterozygote mutants

had normal levels of *Tor* transcript (Figure 4b), even though *Tor* message levels were successively reduced in heterozygous and homozygous $Tor^{MB07988}$ mutant flies (Figure 4b).

To test the effect of *Mtor* inactivation on *Cdc73* expression in a mammalian model, the expression of parafibromin in several tissues harvested from wild-type and *Mtor* heterozygous mice was compared by quantitative immunoblotting. In several tissues examined, including pancreas, liver, and kidney, the expression of parafibromin was reduced in *Mtor* heterozygous mice relative to β-actin (Supplementary Figure S1).

The translational repressor 4E-BP (eIF4EBP), which competes with eIF-4G for binding to eIF-4E to regulate translational initiation,[35] is a downstream target of the Tor kinase in mammals[28] and in flies.[36] As our results indicate an interaction between *hyx* and *Tor* at the transcriptional level, we looked for a possible interaction between *hyx* and *Thor*, the fly ortholog of *EIF4EBP*. Transcript levels of *Thor/EIF4EBP* are reduced by $\sim$50% in *hyx* heterozygotes ($hyx^{EY6898}/+$) (Figure 4c). This reduction in *Thor/EIF4EBP* expression was reversed by the GAL4-induced overexpression of *hyx* (Figure 4c). The level of *Thor/EIF4EBP* transcript in flies expressing the *act5C-Gal4* driver alone was comparable to the controls (Figure 4d). The level of *Thor/EIF4EBP* transcript was reduced by $\sim$30% in *Tor* heterozygotes and additionally reduced to $\sim$50% in double *hyx/Tor* heterozygotes, a reduction rescued by overexpression of *hyx* through the hyx^{EY6898} allele (Figure 4e). Heterozygosity of *hyx* had no effect on the expression of *S6k*, the fly ortholog of *RPS6KB1* encoding the ribosomal protein S6 kinase, another well-characterized downstream target of the Tor kinase in mammals[37] and in flies[36] (Figure 4f).

Next the effect of starvation on relevant transcript levels in control and mutant flies was determined (Figures 5a–e). Although starvation of flies had no effect on *Tor* transcript levels (Figure 5a), *hyx* expression was increased (Figure 5b). The induction of *hyx* by starvation persisted in *Tor* heterozygotes, suggesting nutritional cues may regulate *hyx* transcription independently of *Tor* activity (Figure 5c). Starvation also increased *Thor/EIF4EBP* transcript expression compared with fed controls; however, the level of *Thor/EIF4EBP* transcript in starved *hyx* heterozygous flies was reduced by $\sim$80% compared with starved w^{1118} controls (Figure 5d). There was no difference in the basal *Thor/EIF4EBP* transcript level between w^{1118} control and *Mnn1* heterozygous flies, although the level of starvation-induced *Thor/EIF4EBP* was somewhat lower in the *Mnn1* mutants (Figure 5e). These results suggest that the starvation resistance of both *hyx* and *Tor* heterozygous flies results, at least in part, from impaired upregulation of *Thor/EIF4EBP* in response to caloric deprivation.

To look for these interactions in human cellular models, the effect of serum starvation on the expression of *CDC73* and the three mammalian *EIF4EBP* isoforms was determined in HEK293 human embryonic kidney cells and cultured human peripheral blood mononuclear cells (WBC). Serum starvation for 48 h significantly increased *CDC73, EIF4EBP1*, *EIF4EBP2*, and *EIF4EBP3* transcript expression in HEK293 cells (Figures 5f–i). In control WBC, as in HEK293 cells, serum starvation significantly increased *CDC73* transcript expression (Supplementary Figure S2).

The expression of *EIF4EBP* isoforms was compared in WBC collected from normal healthy volunteer controls and from patients with the HPT-JT (*CDC73* heterozygotes) or MEN1 (*MEN1* heterozygotes) (Supplementary Table S1). Compared with control WBC, basal levels of all three *EIF4EBP* isoforms were reduced in *CDC73* heterozygotes with the most striking reduction in *EIF4EBP3* (Figure 6). In WBC from *MEN1* heterozygous patients, the basal level of *EIF4EBP1* transcript was reduced compared with control; however, there was no difference in the basal *EIF4EBP2* level, and basal *EIF4EBP3* was increased (Figure 6). Serum starvation-induced levels of *EIF4EBP1* and *EIF4EBP2*

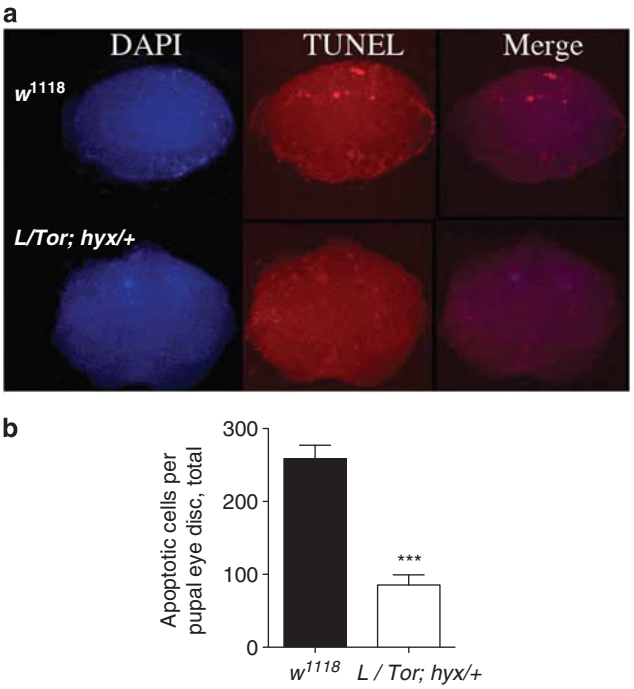

Figure 2 Loss of normal apoptosis during pupal development correlates with the NOG eye phenotype observed in the *L/Tor;hyx* triple heterozygous mutant flies. Normal eye development in *Drosophila* involves a wave of cellular apoptosis between 35 and 50 h after pupal formation (APF) that eliminates a large fraction of undifferentiated interommatidial cells. The eye discs of $L^{si}/Tor^{MB07988}$ $hyx^{EY6898}/+$ triple heterozygotes with a propensity to later develop the NOG phenotype were characterized by a substantial reduction in this usual burst of apoptosis APF compared with w^{1118} controls. (**a**) 4′,6-diamidino-2-phenylindole nuclear staining (left), TUNEL analysis (middle), and merged images (right) of pupal eye discs dissected ~45 h APF reveal a loss and mis-localization of apoptotic-positive cell nuclei in $L^{si}/Tor^{MB07988}$ $hyx^{EY6898}/+$ triple heterozygote flies compared with w^{1118} controls. The difference in size between w^{1118} control and $L^{si}/Tor^{MB07988}$ $hyx^{EY6898}/+$ triple heterozygote eye discs shown represents a random variation and was not reflective of a consistent difference between the two. (**b**) Quantification of apoptotic cells per pupal eye disc shows significant (~60%) reduction in total apoptotic-positive cell nuclei in $L^{si}/Tor^{MB07988}$ $hyx^{EY6898}/+$ triple heterozygotes compared with w^{1118} controls (***$P<0.0001$, unpaired Student's *t*-test; w^{1118} control, $n=16$; $L^{si}/Tor^{MB07988}$ $hyx^{EY6898}/+$, $n=18$)

transcript did not discriminate between *CDC73* and *MEN1* heterozygous patients, and both groups of patients had lower induced transcript levels than the controls (Figure 6). In contrast, the serum starvation-induced level of *EIF4EBP3* transcript from *CDC73* heterozygous patients was markedly lower than that from both control and *MEN1* heterozygous patient WBCs (Figure 6). Thus, reduced basal and serum starvation-induced *EIF4EBP3* transcript in peripheral WBC represents a phenotype that correlates strongly with *CDC73* heterozygosity, but not with that of *MEN1*.

Chromatin immunoprecipitation (ChIP) was used in HEK293 cells to determine if the effect of *CDC73* allele dosage on *EIF4EBP3* transcript levels was consistent with regulation at the transcriptional level. Three pairs of primers were used to interrogate anti-parafibromin immunoprecipitates in a ChIP assay by quantitative PCR, with one primer set (P1) targeting the upstream *EIF4EBP3* promoter region, one set (P2) targeting the internal gene coding sequence at exon 2, and one set (P3) directed at a flanking region downstream of the putative poly A signal (Figure 7a). Antibodies to other components of the PAF1 complex, Leo1, and Paf1 were also used. As shown in Figure 7b, primer pairs P1 and P2 produced significantly higher signals from the anti-parafibromin, anti-Leo1, and anti-Paf1 immunoprecipitates than from those using control IgG. The specific anti-parafibromin ChIP signal was much stronger in the P1 and P2 regions of *EIF4EBP3* than in the P3 region, and no signal at all was detectable in the P3 region with anti-Leo1 or anti-Paf1 ChIP (Figure 7b). Taken together, these data suggest that the PAF1 complex might be involved in both *EIF4EBP3* transcript initiation and elongation, consistent with PAF1 complex function at other gene loci.[12–14,38]

Discussion

Gene expression profiling studies of parathyroid tumors by Haven *et al*.[39] strongly suggest that sporadic parathyroid malignancies and tumors associated with *CDC73* inactivation follow a pathway distinct from benign sporadic and *MEN1*-related parathyroid tumors. This dichotomy is reinforced by the clinical observations that inactivation of *CDC73* is frequent in parathyroid cancer,[8,9] but rare in sporadic benign parathyroid tumors,[16,17] whereas mutation of *MEN1* is nearly always associated with benign parathyroid adenomas in both sporadic and MEN1-associated cases.

We show here that *EIF4EBP3* is distinctly regulated by *CDC73* and *MEN1*, that parafibromin and other PAF1 complex components occupy the *EIF4EBP3* promoter and coding regions, and that loss of *EIF4EBP3* expression represents a marker of *CDC73* haploinsufficiency and heterozygosity, but not *MEN1* loss-of-function, in a human WBC model system. As current PCR-based *CDC73* germline mutation testing methods may miss some carriers,[7] our results indicate it may be possible to independently assess *CDC73* allele dosage by the determination of *EIF4EBP3* expression in a clinically practical manner.

The strong evolutionary conservation of the link between *EIF4EBP* and *CDC73* is striking. Taken together with our previous finding that *hyx* opposes *lobe/Akt1S1* in the eye phenotype assay,[24] the present work strengthens the notion that *TOR* and *CDC73* interact with an overlapping set of regulators and effector targets. Functioning as a sensor of nutrient availability, the protein kinase mTOR regulates cell growth and autophagy.[26] Under physiological conditions, growth signals acting through mTOR promote the phosphorylation of eIF4EBP and reduce its affinity for eIF-4E; thus initiating protein synthesis from a pool of transcripts critical for cell growth and survival. Under pathological conditions, the enhanced function of eIF-4E, frequently a result of inactivation of eIF4EBP by mTor phosphorylation, is linked to poor prognosis and metastasis in multiple malignancies.[30–33] Unlike the inactivation of eIF4EBP by phosphorylation, via the canonical mTOR pathway, loss of *CDC73* exerts its negative effect on *EIF4EBP3* through loss of gene expression. Our findings suggest a model in which de-repression of cap-dependent protein translation and heightened survival resulting from *CDC73* loss-of-function may enhance carcinogenesis in parathyroid tumors, conferring selective advantage

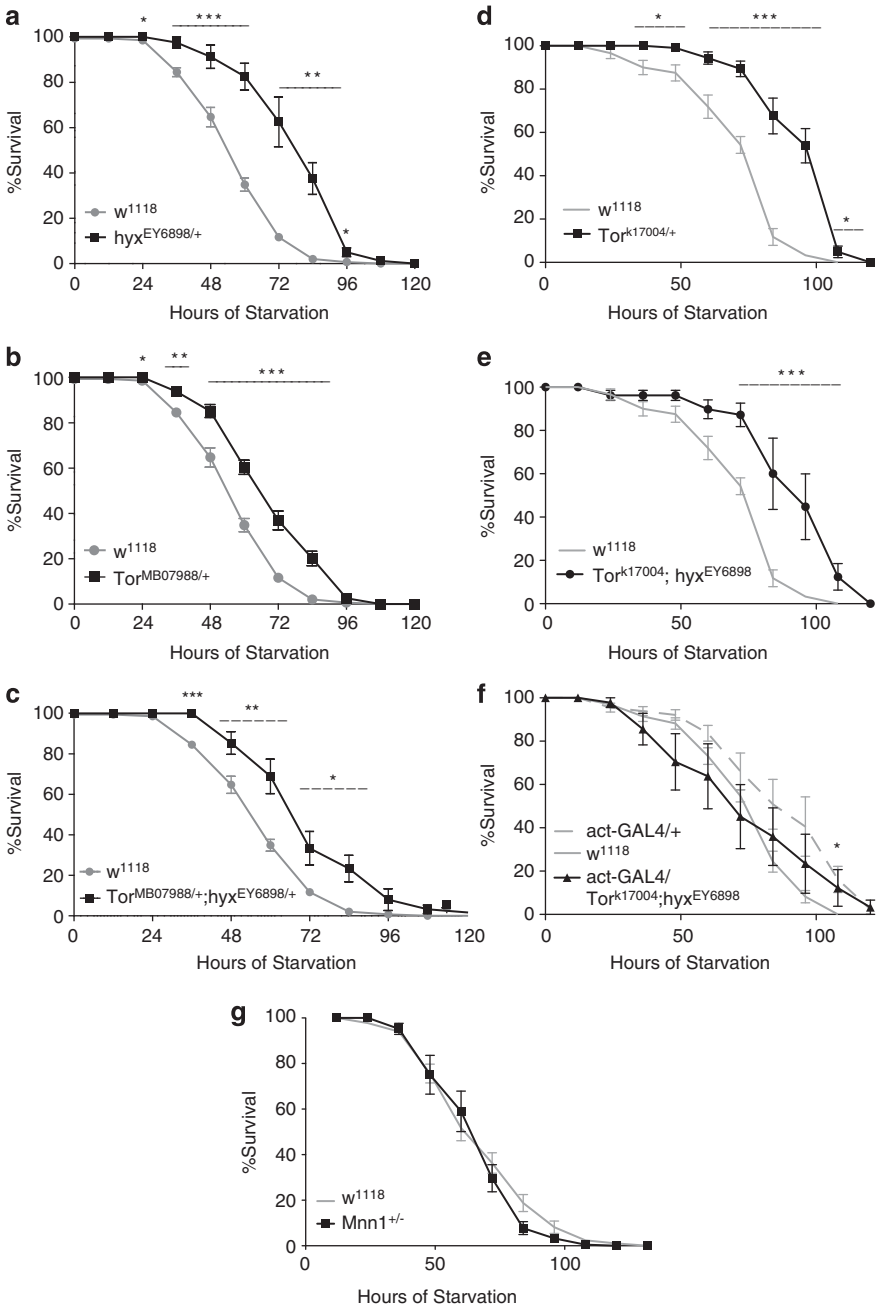

Figure 3 Enhanced starvation resistance in *hyx/CDC73* and *Tor* mutant flies. Survival upon starvation of the indicated single or double *hyx/CDC73* and *Tor* heterozygous mutant fly strains is shown. Flies **a**–**g** were supplied only with water to test starvation resistance. The number of surviving flies was recorded every 12 h. For each experiment, 20 or more vials were used and two or more independent experiments were conducted for each fly line. Vials contained 10 flies each. Each data point represents the pooled mean survival from 20 to 30 vials of the indicated genotype (*$P<0.05$; **$P<0.001$; ***$P<0.0001$; *versus* wt for the indicated time points, two–tailed *P*-values for unpaired Student's *t*-test). The experiment shown in (**f**) tested the rescue of the starvation resistance of the $Tor^{K17004}/+$; $hyx^{EY6898}/+$ double mutant (cf. **e**) by overexpression of *hyx* from the hyx^{EY6898} allele upon mating with a driver strain expressing *GAL4* from the *5C-actin* promoter (*act-GAL4*), with the driver-only control shown (*act-GAL4/+*; dashed gray line). In panel **f**, the *P* values for the unpaired Student's *t*-test comparing the % survival of w^{1118} control strain with the *act-Gal4*/$Tor^{K17004}/+$; $hyx^{EY6898}/+$ strain were: 84 h, $P=0.32$; 96 h, $P=0.14$; 108 h, $P=0.036$

to hypermetabolic neoplastic cells for clonal expansion in the face of nutritional stress.

Materials and Methods

Human subjects. All patients participated in the protocols approved by the Investigational Review Boards of the National Institute of Diabetes and Digestive and Kidney Diseases and each gave written consent. Normal volunteers had no personal or family history of hyperparathyroidism, HPT-JT, or MEN1. Patients with HPT-JT or MEN1 had documented heterozygous germline mutation of *CDC73/HRPT2* or *MEN1*, respectively. Patient characteristics are summarized in Supplementary Table 1.

Fly stocks. The enhancer trapped fly lines from the Japanese NP Consortium Gal4 Enhancer Trap Insertion Database were obtained from the Drosophila Genetic

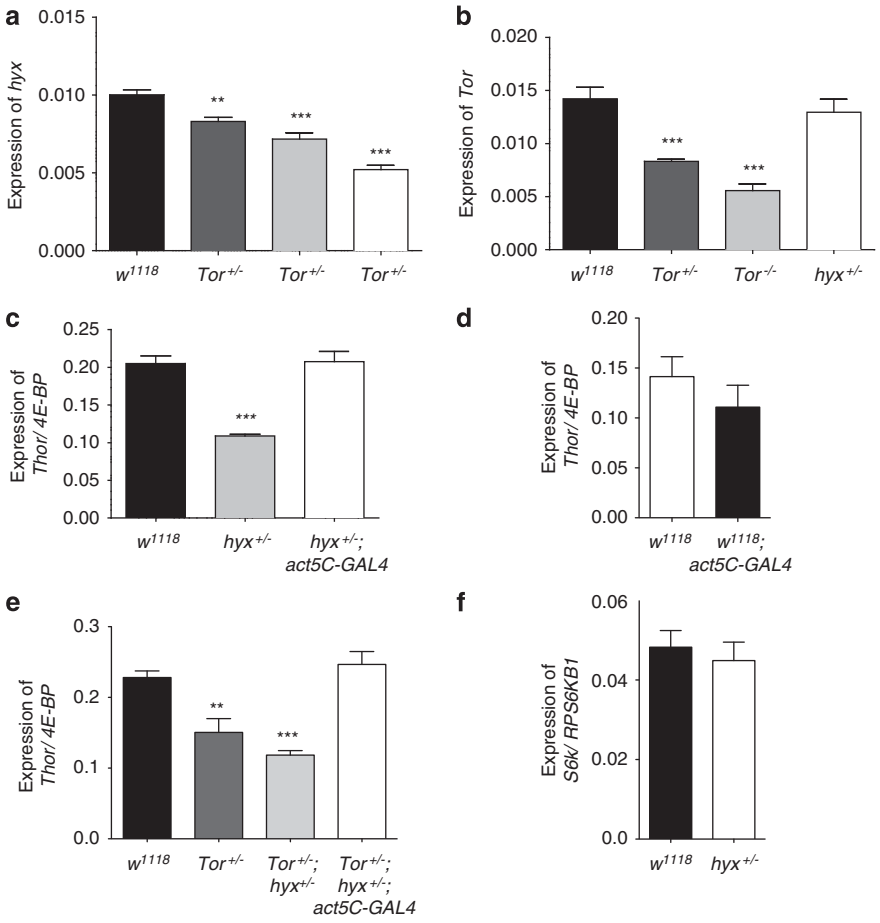

Figure 4 Transcriptional regulation of *Tor*, *hyx*, and *Thor* in fly. Heterozygous $Tor^{+/-}$ ($Tor^{MB07988}/+$) and homozygous $Tor^{-/-}$ ($Tor^{MB07988/MB07988}$) mutant flies have a dose-dependent reduction in both *Tor* and *hyx* transcript compared with w^{1118} controls (**a** and **b**). Heterozygous *hyx* ($hyx^{EY6898}/+$) mutant flies show a reduction in *hyx,* but not in *Tor* transcript expression (**a** and **b**). *Thor/4E-BP* transcript expression is significantly reduced in *hyx/CDC73*$^{+/-}$ flies compared with w^{1118} controls, and is rescued back to control levels following *act5C-GAL4*-driven overexpression of *hyx/CDC73* from the hyx^{EY6898} allele (**c**). The *act5C-GAL4*/+ driver alone has no effect on *Thor/4E-BP* transcript levels (**d**). $Tor^{+/-}$ heterozygosity and $Tor^{+/-}$;$hyx^{+/-}$ double heterozygosity results in a decrease in *Thor/4E-BP* transcript levels, and is similarly rescued following *act5C-GAL4*-driven overexpression of *hyx/CDC73* from the hyx^{EY6898} allele in the $Tor^{+/-}$;$hyx^{+/-}$ double heterozygous mutant background (**e**). Heterozygosity of *hyx/CDC73*$^{+/-}$ has no effect on transcript levels of *s6k/RPS6KB1*, which is, like 4E-BP, a major effector of Tor (**f**). For **a**, **b**, **c**, and **e** $^{**}P<0.005$; $^{***}P<0.0005$ compared with w^{1118} control, using unpaired Student's *t*-test

Resource Center, Kyoto Institute of Technology (Kyoto, Japan). The fly line bearing the hypomorphic allele, hyx^{EY6898}, which contains a P-element (P[EPgy2]) insertion located 36 bp upstream of the *hyx* translational start site in the 5′ untranslated transcript region (Stock No. 16768), and all the other fly lines used, including $Mnn1^{DG30701}$ (Stock No. 21335), Tor^{K17004}/CyO (Stock No. 11218), $Tor^{MB07988}$ (Stock No. 25363), and Act5C-GAL4/CyO (Stock no. 4414), were from the Bloomington Drosophila Stock Center at Indiana University (Bloomington, IN, USA).

Scanning electron microscopy. Flies were fixed in 4% paraformaldehyde (Electron Microscopy Sciences, Hatfield, PA, USA). Before examination, the samples were dehydrated through 100% ethanol, and then critically point dried (Tousimis model Samdri-795, Rockville, MD, USA). A 10-nm gold coating was deposited in a sputter coater (Electron Microscopy Sciences model 575 ×), and the detailed structure of the fly eyes were studied at 5 kV on a scanning electron microscope (Hitachi S-3400N, Pleasanton, CA, USA).

Pupal eye disc apoptosis analysis. The ApopTag Red *In situ* Apoptosis Detection Kit (Millipore, Billerica, MA, USA) was used for TUNEL analysis. Eye discs collected ∼45 h following pupation were dissected in PBS and analyzed for apoptosis following the same method as previously described for the eye discs of third instar fly larvae.[24]

Fly starvation resistance. For starvation stress tests, flies with desired genotypes that eclosed within 24 h were collected. After ageing for 8 days at 25°C, mated female flies were placed into vials containing paper discs ($d=2.3$ cm) soaked in 400 μl of H_2O (Whatman, Piscataway, NJ, USA). H_2O was replenished throughout the experiment as needed. A total of 20–30 vials (10 flies per vial) were used for each test, and at least two independent experiments were performed. Dead flies were recorded every 12 h. For data analysis, each vial was treated as a data point.

mRNA quantification. Gene expression levels were estimated on the basis of the transcript abundance as measured by quantitative RT-PCR. Quantitative RT-PCR was performed with one-step quantitative RT-PCR master mix (Agilent Technologies, Santa Clara, CA, USA) using a Stratagene MX 3005P real time PCR machine (Agilent Technologies) and analyzed using the accompanying software. Each reaction was conducted in triplicate and three to nine biological samples prepared independently were used in data analysis. The Prism software version 5.0c (GraphPad Software, Inc., La Jolla, CA, USA) was used for graphing the analyzed data set. Total RNA was prepared from both mutant and control samples using QIAGEN RNeasy kit (Valencia, CA, USA). Primer sequences were developed using PrimerQuest software (Integrated DNA Technologies, Coralville, IA, USA), and were as follows: *Drosophila Tor* forward (5′-TGG CAA AGC AAC TGG GCA AGA A-3′) and reverse (5′-TCG GGA TCC ACA ATG CGA TGT T-3′); *hyx* forward (5′-TTT GCG TGC CAT CCT GGA CTA T-3′) and reverse (5′-TCT TGC CCG TGC TTT GCA GAA T-3′); *Mnn1* forward (5′-CAA ATG GAT AGA CGG ACT GCT CGT-3′) and reverse (5′GTC AAC AGT TCG TAA CAA GGA TTT GC-3′); *Thor* forward

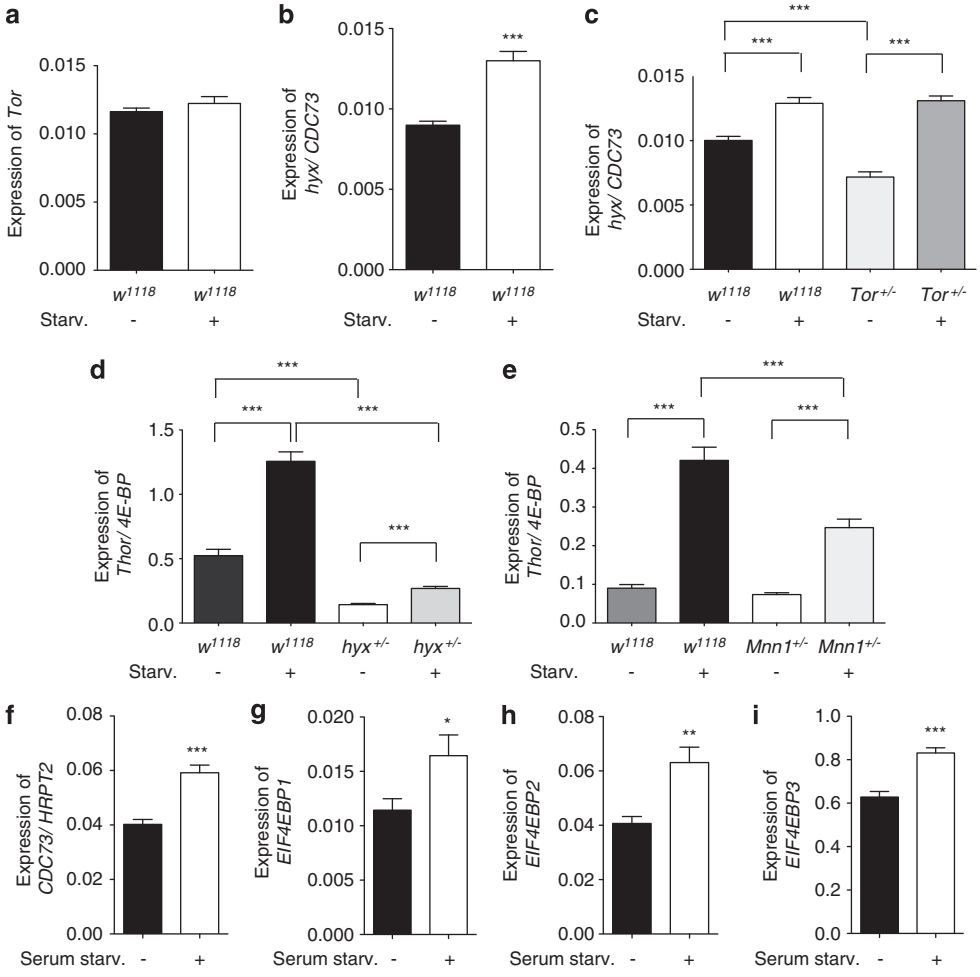

Figure 5 Transcriptional regulation of *hyx/CDC73* and *Thor/4E-BP* in response to caloric or serum starvation. Upregulation in w^{1118} control or mutant flies of *hyx/CDC73* and *Thor/4E-BP*, but not of *Tor* transcript, compared with fed controls following 48 h of starvation (**a**–**d**). The basal reduction of *hyx* transcript observed in $Tor^{+/-}$ ($Tor^{MB0798}/+$) heterozygous flies was lost following 48 h of starvation, suggesting that nutritional cues may regulate *hyx* transcription independently of *Tor* activity (**c**). Conversely, the basal reduction in *Thor/4E-BP* transcript observed in $hyx^{+/-}$ heterozygous flies persists following 48 h of starvation, suggesting that *hyx* is necessary for the starvation-induced increase in *Thor/4E-BP* transcript (**d**). Basal expression of *Thor/4E-BP* transcript was unchanged in $Mnn1^{+/-}$ ($Mnn1^{DG30701}/+$) heterozygous flies compared with w^{1118} controls; however, the level of *Thor* transcript was somewhat reduced following 48 h of starvation (**e**). Expression of human *CDC73*, *EIF4EBP1*, *EIF4EBP2*, and *EIF4EBP3* transcript was significantly increased in HEK293 cells following 48 h of serum starvation (**f–i**). For **b–i** $^*P<0.05$, $^{**}P<0.005$; $^{***}P<0.0005$ compared with control, using unpaired Student's *t*-test

(5′-CCA TGA TCA CCA GGA AGG TTG TCA-3′) and reverse (5′-TCT TCA TGA AAG CCC GCT CGT AGA-3′); *s6k* forward (5′-ATG CGG CGG CTG TTC AAA TAC A-3′) and reverse (5′-TGG CAC TTT CGC TTA GCG TTG T-3′). Human *CDC73* forward (5′-AGA TGC AAC CAG GGG GCA CTG-3′) and reverse (5′-GCA GGA CCC TGC ACA AAA ACG G-3′); *EIF4EBP1* forward (5′-TGG ACA AGA ACG AAC CCT TCC T-3′) and reverse (5′-AGG GAG CTT TCC CAA GCA CAT-3′); *EIF4EBP2* forward (5′-TTT GCA TTC ACC CTC CTT CCC A-3′) and reverse (5′-AGG GCA CCA AAT CCA ACC AGA A-3′); *EIF4EBP3* forward (5′-AAG TTC CTG CTG GAG TGC AAG A-3′) and reverse (5′-TCT CCT GCT CCT TCA GCT CCT C-3′).

Immunoblotting and infrared imaging. Tissues from 6-week old female wild-type C57BL/6 and *Mtor* heterozygous mice (Jackson Laboratory, Bar Harbor, ME, USA, strain B6.129S5-*Mtor*$^{Mtor^{Gt(OST92090)Lex}}$/J, Stock No. 013190) were stored at -80° and then thawed on ice. For every 50 mg of mouse tissue, 1 ml of 1 × RIPA cell lysis buffer (Cell Signaling, Beverly, MA, USA, Cat. No. 9806) including 1 × protease inhibitors (Calbiochem, EMD Serono, Inc., Rockland, MA, USA, Cat. No. 539134) was added followed by homogenization on ice in a 1.5-ml microcentrifuge tube using a tissue homogenizer (Omni International, Kennesaw, GA, USA, Model TH-115) at high speed for 30 s. Homogenates were combined with an equal volume of Laemmli's 2 × gel loading buffer, vortexed, and heated at 95°C for 10 min before gel loading. Electrophoresis by SDS-PAGE was followed by the transfer of the proteins on to 0.45-micron nitrocellulose membrane. Membranes were blocked with TBS or PBS (pH 7.4) containing 0.1% Tween 20 and 5% nonfat dry milk (blocking buffer), and incubated overnight with primary antibodies in the same buffer. Primary antibodies used were rabbit anti-parafibromin polyclonal (GRAPE antibody[40]) and mouse monoclonal anti-β- actin (Sigma-Aldrich, St. Louis, MO, USA, Cat. No. A5316). Membranes were then washed, and IR-labeled secondary antibodies (dilution 1 : 20 000) were used for detecting the protein signals in conjunction with the Odyssey infrared imaging system (LI-COR Biosciences, Lincoln, NE, USA). Quantification of parafibromin immunoreactivity used the β-actin signal in the same lane for normalization. IR secondary antibodies (anti-rabbit IR 800 and anti-mouse Green) were from LI-COR Biosciences.

Mammalian cell culture. Human embryonic kidney HEK293 cells (American Type Culture Collection, Manassas, VA, USA, Cat. No. CRL-1573) were grown in 75-cm^2 flasks in DMEM supplemented with 10% fetal bovine serum (FBS), 4 mM L-glutamine and penicillin/streptomycin at 37°C and 5% CO2. For serum-starvation experiments, HEK293 cells newly seeded the night before were either fed with medium supplemented with 10% FBS (control) or not (starved) for 48 h. Cells were then detached using Trypsin–EDTA, pelleted in microcentrifuge tubes, and either used immediately or stored at -80°C.

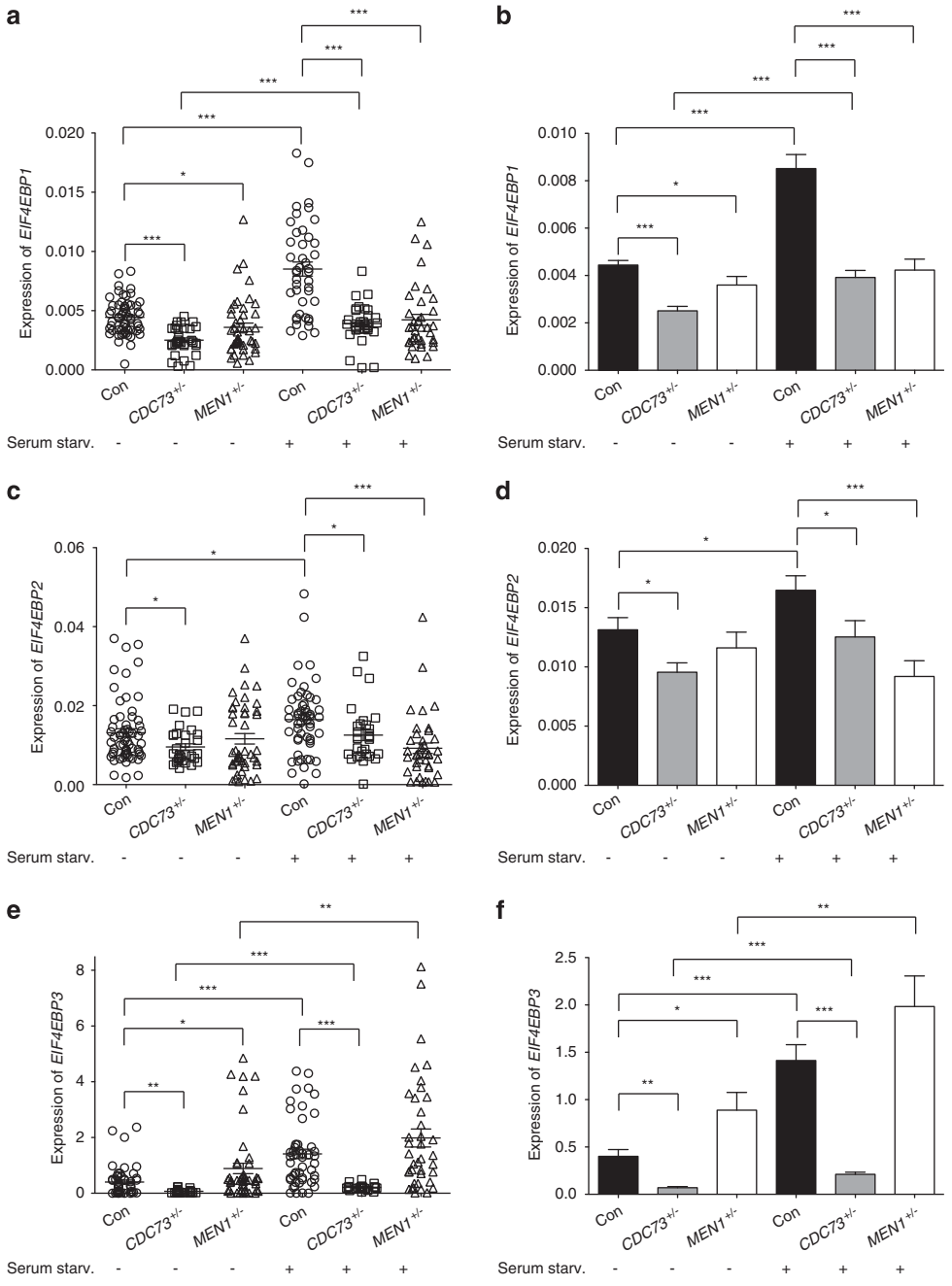

Figure 6 Heterozygosity of *CDC73* results in a reduction of *EIF4EBP* transcript levels in human WBCs. WBCs were collected from healthy volunteers or from patients with HPT-JT (*CDC73* heterozygotes) or MEN1 (*MEN1* heterozygotes). The expression of transcripts for the indicated isoforms of *EIF4EBP* was determined by quantitative RT-PCR following 72 h of control culture conditions or serum starvation, as indicated. The same data are presented as scatter dot plots on the left (**a**, **c** and **e**) and histograms on the right (**b**, **d** and **f**). Control, $n = 43$–62 transcript measurements from eight cell harvests from eight normal volunteers. $CDC73^{+/-}$, $n = 22$–34 transcript measurements from seven cell harvests from five patients. $MEN1^{+/-}$, $n = 37$–47 transcript measurements from 11 cell harvests from 9 patients. For **a–f** $^{*}P < 0.05$, $^{**}P < 0.005$; $^{***}P < 0.0005$ for indicated comparisons, using unpaired Student's *t*-test

A mononuclear cell fraction was isolated from a morning whole blood sample drawn from non-fasting normal volunteers, *CDC73* or *MEN1* heterozygotes (collected at room temperature in heparinized tubes) processed using Lymphocyte Separation Medium (Lonza, Walkersville, MD, USA, Cat. No. 17–829E). The buffy layer, enriched in lymphocytes and mononuclear cells, was collected, washed once in PBS after which the cells were resuspended in complete RPMI medium 1640 (GIBCO, Life Technologies, Grand Island, NY, USA) containing 10% FBS, plated on to 12-well cell culture plates and incubated at 37°C with 5% CO_2. After 24 h of incubation, non-adherent cells were gently removed and the adherent cell population, enriched in mononuclear cells, was divided and further incubated with either fresh complete RPMI medium (control cells) or the RPMI medium without serum (serum-starved cells) for an additional 72 h. The cells were then detached by trypsin–EDTA treatment, pelleted in microcentrifuge tubes, and stored at −80°C until use.

ChIP assay. ChIP assay kit from Millipore (Cat. No. 17–295) was used in the analysis of HEK293 cells following the manufacturer's instructions except that the QIAquick PCR purification kit (Qiagen, Cat. No. 28104) was used for DNA purification. Purified DNA was used as a template for the amplification of selected

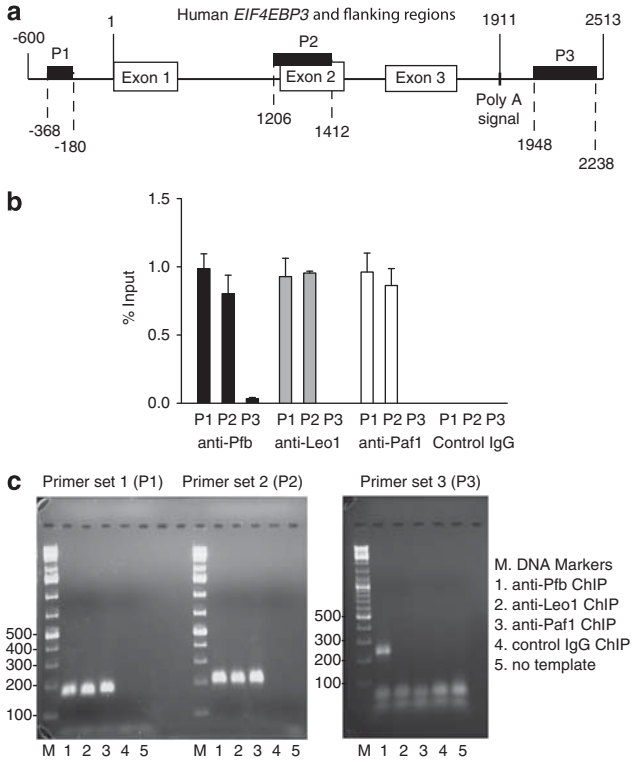

Figure 7 ChIP demonstrates occupancy at *EIF4EBP3* by the PAF1 complex. The physical association of endogenous parafibromin and other components of the PAF1 complex (including the Paf1 and Leo1 proteins) with human *EIF4EBP3* was examined by ChIP in HEK293 cells. (**a**) Schematic diagram showing the relative location of the three PCR primer sets used in the ChIP assay (P1, P2, and P3) along the human *EIF4EBP3* gene (HGNC ID: 3290) and flanking regions (not to scale). The numbering shown is relative to the first base of exon 1 as $+1$ as indicated. (**b**) ChIP analysis using primer sets targeting upstream (P1), exon 2 (P2) and downstream (P3) sequence of *EIF4EBP3* using antibodies against parafibromin, Leo1 or Paf11 or control rabbit IgG as shown. Results shown are mean percentage of input signal ± S.E.M. (**c**) Qualitative analysis of ChIP PCR-derived DNA products by agarose gel electrophoresis and ethidium bromide staining. All experiments are representative of three or more independent biological repeats

regions of *EIF4EBP3* and its flanking sequences using the following primer pairs (Figure 7a): P1 (upstream promoter region, PCR product 191 bp, forward 5′-TCC CTT CCT GCA AGA TGT GTG ACT-3′, reverse 5′-TGG CCC AGC GCT GGC CAA CCT GCC-3′); P2 (exon 2 region, PCR product 206 bp, forward 5′-TCC TGA CTC TTA CCT CAG TCC CAA-3′, reverse 5′-TAC CGG GTA TCT CTT CCT CTG TCT-3′); P3 (downstream region following putative polyA signal, PCR product 288 bp, forward 5′-TCT CAT CTC AGC CAC ACA GCT GAA-3′, reverse 5′-ATA GGC TGG GAC AGC ACC TCT T-3′). Antibodies used for the ChIP assay were anti-parafibromin (GRAPE antibody[40]), anti-Leo1 (Bethyl Laboratories, Montgomery, TX, USA, Cat. No. A300-175A) and anti-Paf1 (Upstate (Millipore), Cat. No. 07–653), and control rabbit IgG (Santa Cruz Biotechnologies, Santa Cruz, CA, USA, Cat. No. sc-2027). Real-time quantitative PCR was performed using 2 × Brilliant II SYBR green QPCR master mix (Agilent Technologies, Cat. No. 600828-51) using the Stratagene Mx3005P QPCR system. PCR parameters used were 95°C 10 min, 40 cycles of 94°C 30 s, 60°C 1 min, and 72°C 1 min, followed by 1 cycle of dissociation curve analysis. The size and quality of the PCR-amplified DNA was assessed by agarose gel electrophoresis and ethidium bromide staining in comparison to DNA markers (GeneRuler DNA Ladder Mix, Fermentas, Glen Burnie, MD, USA, Cat. No. SM0333). Data analysis and graphing were performed using Prism software version 5.0c (GraphPad Software, Inc.) with results expressed as percentage input signal after normalizing Ct values from each primer set.

Statistical analysis. Data were analyzed by Prism software version 5.0c. (GraphPad Software, Inc.). Unpaired Student's *t*-test was used to evaluate for statistical significance.

Conflict of Interest

The authors declare no conflict of interest.

Acknowledgements. We are grateful to Sunita Agarwal and Stephen Marx for encouragement and helpful discussions. This research was supported by the Intramural Research Programs of the National Institute of Diabetes and Digestive and Kidney Diseases, the National Heart, Lung and Blood Institute, and the National Institute of Allergy and Infectious Diseases.

1. Jackson CE, Norum RA, Boyd SB, Talpos GB, Wilson SD, Taggart RT *et al.* Hereditary hyperparathyroidism and multiple ossifying jaw fibromas: a clinically and genetically distinct syndrome. *Surgery* 1990; **108**: 1006–1012.
2. Mallette LE, Malini S, Rappaport MP, Kirkland JL. Familial cystic parathyroid adenomatosis. *Ann Intern Med* 1987; **107**: 54–60.
3. Teh BT, Farnebo F, Kristoffersson U, Sundelin B, Cardinal J, Axelson R *et al.* Autosomal dominant primary hyperparathyroidism and jaw tumor syndrome associated with renal hamartomas and cystic kidney disease: linkage to 1q21-q32 and loss of the wild type allele in renal hamartomas. *J Clin Endocrinol Metab* 1996; **81**: 4204–4211.
4. Teh BT, Farnebo F, Twigg S, Höög A, Kytölä S, Korpi-Hyövälti E *et al.* Familial isolated hyperparathyroidism maps to the hyperparathyroidism-jaw tumor locus in 1q21-q32 in a subset of families. *J Clin Endocrinol Metab* 1998; **83**: 2114–2120.
5. Simonds WF, James-Newton LA, Agarwal SK, Yang B, Skarulis MC, Hendy GN *et al.* Familial isolated hyperparathyroidism: Clinical and genetic characteristics of thirty-six kindreds. *Medicine (Baltimore)* 2002; **81**: 1–26.
6. Simonds WF, Robbins CM, Agarwal SK, Hendy GN, Carpten JD, Marx SJ. Familial isolated hyperparathyroidism is rarely caused by germline mutation in HRPT2, the gene for the hyperparathyroidism-jaw tumor syndrome. *J Clin Endocrinol Metab* 2004; **89**: 96–102.
7. Carpten JD, Robbins CM, Villablanca A, Forsberg L, Presciuttini S, Bailey-Wilson J *et al.* HRPT2, encoding parafibromin, is mutated in hyperparathyroidism-jaw tumor syndrome. *Nat Genet* 2002; **32**: 676–680.
8. Shattuck TM, Valimaki S, Obara T, Gaz RD, Clark OH, Shoback D *et al.* Somatic and germline mutations of the HRPT2 gene in sporadic parathyroid carcinoma. *N Engl J Med* 2003; **349**: 1722–1729.
9. Cetani F, Pardi E, Borsari S, Viacava P, Dipollina G, Cianferotti L *et al.* Genetic analyses of the HRPT2 gene in primary hyperparathyroidism: germline and somatic mutations in familial and sporadic parathyroid tumors. *J Clin Endocrinol Metab* 2004; **89**: 5583–5591.
10. Wade PA, Werel W, Fentzke RC, Thompson NE, Leykam JF, Burgess RR *et al.* A novel collection of accessory factors associated with yeast RNA polymerase II. *Protein Expr Purif* 1996; **8**: 85–90.
11. Shi X, Chang M, Wolf AJ, Chang CH, Frazer-Abel AA, Wade PA *et al.* Cdc73p and Paf1p are found in a novel RNA polymerase II-containing complex distinct from the Srbp-containing holoenzyme. *Mol Cell Biol* 1997; **17**: 1160–1169.
12. Rozenblatt-Rosen O, Hughes CM, Nannepaga SJ, Shanmugam KS, Copeland TD, Guszczynski T *et al.* The parafibromin tumor suppressor protein is part of a human Paf1 complex. *Mol Cell Biol* 2005; **25**: 612–620.
13. Yart A, Gstaiger M, Wirbelauer C, Pecnik M, Anastasiou D, Hess D *et al.* The HRPT2 tumor suppressor gene product parafibromin associates with human PAF1 and RNA polymerase II. *Mol Cell Biol* 2005; **25**: 5052–5060.
14. Zhu B, Mandal SS, Pham AD, Zheng Y, Erdjument-Bromage H, Batra SK *et al.* The human PAF complex coordinates transcription with events downstream of RNA synthesis. *Genes Dev* 2005; **19**: 1668–1673.
15. Mosimann C, Hausmann G, Basler K. Parafibromin/Hyrax activates Wnt/Wg target gene transcription by direct association with beta-catenin/Armadillo. *Cell* 2006; **125**: 327–341.
16. Krebs LJ, Shattuck TM, Arnold A. HRPT2 mutational analysis of typical sporadic parathyroid adenomas. *J Clin Endocrinol Metab* 2005; **90**: 5015–5017.
17. Bradley KJ, Cavaco BM, Bowl MR, Harding B, Cranston T, Fratter C *et al.* Parafibromin mutations in hereditary hyperparathyroidism syndromes and parathyroid tumours. *Clin Endocrinol* 2006; **64**: 299–306.
18. Gagel RF, Marx SJ. Multiple endocrine neoplasia. In: Kronenberg HM, Melmed S, Polonsky KS, Larsen PR (eds) *Williams Textbook of Endocrinology* 11th edn. WB Saunders & Co: Philadelphia, 2007, pp 1705–1746.
19. Heppner C, Kester MB, Agarwal SK, Debelenko LV, Emmert-Buck MR, Guru SC *et al.* Somatic mutation of the MEN1 gene in parathyroid tumours. *Nat Genet* 1997; **16**: 375–378.
20. Farnebo F, Teh BT, Kytola S, Svensson A, Phelan C, Sandelin K *et al.* Alterations of the MEN1 gene in sporadic parathyroid tumors. *J Clin Endocrinol Metab* 1998; **83**: 2627–2630.
21. Wang P, Bowl MR, Bender S, Peng J, Farber L, Chen J *et al.* Parafibromin, a component of the human PAF complex, regulates growth factors and is required for embryonic development and survival in adult mice. *Mol Cell Biol* 2008; **28**: 2930–2940.
22. Lin L, Zhang JH, Panicker LM, Simonds WF. The parafibromin tumor suppressor protein inhibits cell proliferation by repression of the c-myc proto-oncogene. *Proc Natl Acad Sci U S A* 2008; **105**: 17420–17425.
23. Rozenblatt-Rosen O, Nagaike T, Francis JM, Kaneko S, Glatt KA, Hughes CM *et al.* The tumor suppressor Cdc73 functionally associates with CPSF and CstF 3′ mRNA processing factors. *Proc Natl Acad Sci U S A* 2009; **106**: 755–760.

24. Zhang JH, Panicker LM, Seigneur EM, Lin L, House CD, Morgan W *et al.* Cytoplasmic polyadenylation element binding protein is a conserved target of tumor suppressor HRPT2/CDC73. *Cell Death Differ* 2010; **17**: 1551–1565.
25. Sancak Y, Thoreen CC, Peterson TR, Lindquist RA, Kang SA, Spooner E *et al.* PRAS40 is an insulin-regulated inhibitor of the mTORC1 protein kinase. *Mol Cell* 2007; **25**: 903–915.
26. Sengupta S, Peterson TR, Sabatini DM. Regulation of the mTOR complex 1 pathway by nutrients, growth factors, and stress. *Mol Cell* 2010; **40**: 310–322.
27. Robert F, Pelletier J. Translation initiation: a critical signalling node in cancer. *Expert Opin Ther Targets* 2009; **13**: 1279–1293.
28. Mamane Y, Petroulakis E, LeBacquer O, Sonenberg N. mTOR, translation initiation and cancer. *Oncogene* 2006; **25**: 6416–6422.
29. Graff JR, Zimmer SG. Translational control and metastatic progression: enhanced activity of the mRNA cap-binding protein eIF-4E selectively enhances translation of metastasis-related mRNAs. *Clin Exp Metastasis* 2003; **20**: 265–273.
30. Yeh CJ, Chuang WY, Chao YK, Liu YH, Chang YS, Kuo SY *et al.* High expression of phosphorylated 4E-binding protein 1 is an adverse prognostic factor in esophageal squamous cell carcinoma. *Virchows Arch* 2011; **458**: 171–178.
31. Li BD, Liu L, Dawson M, De Benedetti A. Overexpression of eukaryotic initiation factor 4E (eIF4E) in breast carcinoma. *Cancer* 1997; **79**: 2385–2390.
32. Rojo F, Najera L, Lirola J, Jimenez J, Guzman M, Sabadell MD *et al.* 4E-binding protein 1, a cell signaling hallmark in breast cancer that correlates with pathologic grade and prognosis. *Clin Cancer Res* 2007; **13**: 81–89.
33. Castellvi J, Garcia A, Rojo F, Ruiz-Marcellan C, Gil A, Baselga J *et al.* Phosphorylated 4E binding protein 1: a hallmark of cell signaling that correlates with survival in ovarian cancer. *Cancer* 2006; **107**: 1801–1811.
34. Wolff T, Ready DF. Cell death in normal and rough eye mutants of Drosophila. *Development* 1991; **113**: 825–839.
35. Lasko P. Gene regulation at the RNA layer: RNA binding proteins in intercellular signaling networks. *Sci STKE* 2003; **2003**: RE6.
36. Miron M, Lasko P, Sonenberg N. Signaling from Akt to FRAP/TOR targets both 4E-BP and S6 K in *Drosophila melanogaster*. *Mol Cell Biol* 2003; **23**: 9117–9126.
37. Zoncu R, Efeyan A, Sabatini DM. mTOR: from growth signal integration to cancer, diabetes and ageing. *Nat Rev Mol Cell Biol* 2011; **12**: 21–35.
38. Mueller CL, Jaehning JA. Ctr9, Rtf1, and Leo1 are components of the Paf1/RNA polymerase II complex. *Mol Cell Biol* 2002; **22**: 1971–1980.
39. Haven CJ, Howell VM, Eilers PH, Dunne R, Takahashi M, van Puijenbroek M *et al.* Gene expression of parathyroid tumors: molecular subclassification and identification of the potential malignant phenotype. *Cancer Res* 2004; **64**: 7405–7411.
40. Lin L, Czapiga M, Nini L, Zhang JH, Simonds WF. Nuclear localization of the parafibromin tumor suppressor protein implicated in the hyperparathyroidism-jaw tumor syndrome enhances its proapoptotic function. *Mol Cancer Res* 2007; **5**: 183–193.

Supplementary Information accompanies the paper on Cell Death and Disease website (http://www.nature.com/cddis)